Thermophysical Properties of Trehalose and Its Concentrated Aqueous Solutions

Danforth P. Miller,[1] Juan J. de Pablo,[1,3] and Horacio Corti[2]

Received December 30, 1996; accepted February 11, 1997

Purpose. To address the lack of fundamental thermophysical data for trehalose and its aqueous systems by measuring equilibrium and non-equilibrium properties of such systems.

Methods/Results. Differential scanning calorimetry (DSC) and dynamic mechanical analysis were used to measure glass transition temperatures of trehalose and its solutions. X-ray diffractometry was used to verify the structure of amorphous trehalose. Controlled-stress rheometry was used to measure viscosity of several aqueous trehalose systems at ambient and sub-ambient temperatures. Over this temperature range, the density of these solutions was also measured with a vibrating tube densimeter. The equilibrium phase diagram of aqueous trehalose was determined by measuring the solubility and freezing point depression.

Conclusions. Our solubility measurements, which have allowed long times for attainment of chemical equilibrium, are substantially different from those reported earlier that used different techniques. Our measurements of the glass transition temperature of trehalose are higher than reported values. A simple model for the glass transition is presented to describe our experimental observations.

KEY WORDS: trehalose; phase diagram; glass transition; viscosity; molar volume; cryoprotection.

INTRODUCTION

In recent years, aqueous solutions of trehalose have received considerable attention. Trehalose (α-D-glucopyranosyl-α-D-glucopyranoside) is a non-reducing disaccharide of glucose found in several organisms that are able to survive drying (1). The prevalence of trehalose in living organisms that can survive long periods of drought, termed "anhydrobiosis", suggests that trehalose is a particularly effective desiccation protectant. Its ability to protect cells from freezing injury has been widely demonstrated (2,3). Among saccharides, trehalose is particularly effective in terms of its ability to preserve and maintain activity of biomolecules (4); it has been shown to protect various proteins, viruses and antibodies during drying (5,6,7). Its capacity to preserve the contents and structure of liposomes has also been demonstrated (8).

Despite its importance in cryopreservation and desiccation protection, the properties that make trehalose an effective protective agent are still poorly understood. There are several hypotheses that attempt to explain why trehalose is particularly effective, none of which completely accounts for experimental observations. Some "theories" are based upon the interaction of trehalose with biological structures, while others are based solely upon the interaction of trehalose with water and the thermophysical properties of its aqueous solutions. On one hand, Green and Angell (9) have proposed that the higher glass transition temperature (T_g) of the trehalose/water system (compared to that of other glass-forming mono- and disaccharides) could be responsible for its superior protective properties. Further, they have shown that there is a strong correlation between the protective ability of protective agents and their glass transition temperatures. On the other hand, Crowe and coworkers (10) have noted that vitrification is not sufficient for preservation. Vitrification alone does not explain, for example, why another carbohydrate, dextran, which has a significantly higher glass transition temperature than trehalose, is a much less effective cryoprotectant than trehalose.

Crowe and coworkers (4) compiled crystallographic data for several carbohydrates in an attempt to identify correlations between effectiveness at stabilizing membranes and the number and type of hydroxyl groups of the carbohydrate. They found no clear relationship between the effectiveness of the carbohydrate and any of the parameters studied. Unfortunately, these authors had to use the crystal structure as the basis of their investigation since the conformation of the carbohydrate near the membrane was not known. Microscopic arguments for trehalose's effectiveness, based on molecular simulation studies, are inconclusive; much work is needed in that area (11,12).

The idea that trehalose stabilizes biological structures in the absence of water was first proposed by Crowe (13). This idea is an extension of a hypothesis to describe the protective properties of inositol, which was first proposed by Webb (14). The so-called water replacement hypothesis asserts that trehalose hydrogen bonds with the polar headgroups of the lipids that constitute biomembranes. As the system is dried or frozen, these interactions replace those of the water of hydration at the membrane-fluid interface. This helps maintain membrane headgroups at their hydrated spacing (12). The presence of these stabilizing interactions is further supported by findings from calorimetry and NMR spectroscopy of membrane vesicles. Crowe *et al.* (15) found that trehalose prevented phase separation of membrane components during drying and phase transitions during rehydration. Additional findings from heat of solution calorimetry (16) support this concept by inferring hydration numbers for various saccharides in solution. Trehalose was reported to be the most effective hydrogen bond donor among the three disaccharides: trehalose, maltose and sucrose. Note that raffinose, a trisaccharide, was found to be an even more effective hydrogen bond donor than all the others; it is, however, a less effective protective agent than the others (5).

More recently, Aldous and coworkers (17) have suggested that the ability to crystallize a stoichiometric hydrate from the amorphous "phase" lends exceptional stabilization properties to certain carbohydrates often used in lyophilization. This stabilization occurs during long-term storage, where the presence of low concentrations of water is inevitable. In this case, they suggest that the amorphous saccharide is stabilized by incorporation of trace amounts of water into the crystalline dihydrate rather than into the amorphous phase. This prevents water from acting as a plasticizer of the amorphous phase, which would

[1] Department of Chemical Engineering, University of Wisconsin-Madison, 1415 Engineering Drive, Madison, Wisconsin 53706.
[2] Departamento de Química, C.N.E.A. and Instituto de Química de Materiales, Medio Ambiente y Energía, Buenos Aires, Argentina.
[3] To whom correspondence should be addressed.

0724-8741/97/0500-0578$12.50/0

lead to a decrease of T_g. However, the rates of both the crystallization of the hydrate and the migration of water in such concentrated "solutions" have not been examined in detail. Although such processes are thermodynamically favorable, they are kinetically inhibited due to low molecular mobility in the amorphous "phase".

Jasra and Ahluwalia (18) have measured the heat of solution at infinite dilution for several carbohydrates. Interestingly, we notice that for the disaccharides studied, the magnitude of the heat of solution follows the sequence of the relative effectiveness for preserving biological membranes as reported by Crowe *et al.* (4): trehalose dihydrate, lactose monohydrate, maltose monohydrate, cellobiose, and sucrose. This suggests, but does not prove, a relationship between protective ability and the molecular processes that contribute to the heat of solution. The heat of solution of the crystalline dihydrate depends on the stability of the crystal structure. From an energetic standpoint, the energy required to remove the water molecules from the crystal structure gives rise to a large positive heat of solution. In an effort to examine the interaction between amorphous saccharides and water, we are currently measuring the heat of solution of the amorphous forms of the above carbohydrates.

Given the many unanswered questions regarding trehalose's "special" properties, the scarcity of fundamental data in the literature is surprising. Slade and Levine (19) have stated that there is a lack of data for concentrated aqueous solutions of many small carbohydrates, which are of utmost importance in biological and industrial pharmaceutical applications. Data in the dilute regime abound in the literature. These data include the enthalpy of dilution (16), enthalpy of solution (18), the intrinsic viscosity and Huggins (k′) parameters (20,21), and partial molar volume (22–25) of trehalose solutions. Studies in this concentration range provide information about solute-solvent interactions; however, concentrations where solute-solute interactions become important have been largely ignored.

Considering the state of affairs for the trehalose/water system, it is no surprise that ternary systems have been mostly ignored in the literature. The importance of electrolytes in biological systems is undeniable. However, the only reported study (26) of the effects of an electrolyte added to the trehalose/water system is for a freeze-concentrated system. To the best of our knowledge, there have been no other studies of the effect of salts on the T_g of homogeneous trehalose systems. The temperature dependence of molar volume, which ultimately determines the glass transition temperature, of supercooled trehalose solutions has not been measured before. Also, the solubility of trehalose in water has not been measured using methods that allow sufficiently long times to attain chemical equilibrium.

We address these deficiencies by presenting a systematic study of the thermophysical properties of trehalose and its aqueous solutions. These data include non-equilibrium properties such as the temperature dependence of both the density and dynamic viscosity of supercooled systems. These viscosity data are used to assess the fragility of several trehalose/water mixtures. The greatest utility of viscometric and volumetric data lies in their use in models to predict the glass transition temperature. This relationship is natural, since many models view the glass transition as either a free volume phenomenon or an isoviscosity state. We present a simple model for predicting T_g and compare its results to measured values.

We have also measured the glass transition temperature of several trehalose/water mixtures ranging from 60wt% trehalose to dry, amorphous trehalose. These measurements were performed using two different techniques: differential scanning calorimetry (DSC) and dynamic mechanical analysis (DMA). Shalaev and Franks (27) have discussed the differences between the T_g values obtained by both methods, using fructose and sucrose as glass-forming liquids. The use of two independent techniques serves to validate the T_g results presented in this work. Previously, a wide range of glass transition temperatures of amorphous trehalose have been reported (midpoint of transition): 79°C (9); 107°C (28); 115°C (29). This scattering prompted us to prepare amorphous trehalose samples and calorimetrically measure T_g. We have verified that the structure was indeed amorphous by using X-ray diffraction at temperatures just below the measured T_g.

We present the solid-liquid equilibrium phase diagram of trehalose/water mixtures. Green and Angell (9) have determined such a phase diagram by DSC. More recently, Nicolajsen and Hvidt (26) reported the solubility of trehalose in water determined by measuring the temperature at which trehalose precipitates when a saturated solution is cooled. Despite the good agreement between these two groups of authors, we noticed in preliminary assays that the solubility of trehalose dihydrate at room temperature was much lower than that estimated by interpolating the results of the aforementioned authors. That prompted us to measure the solubility in experiments in which a long time (days) of equilibration between the solid and solution was allowed to avoid supersaturation or undersaturation. The results of these measurements differ markedly from literature data.

We have also investigated the effects of a third component on the glass transition and ice recrystallization temperatures of trehalose solutions. In particular, due to its physiological and technological importance, we have examined the trehalose/sodium chloride/water system. Our goal is to identify electrolytes that strongly affect T_g. Of course, the presence of a third component provides many more possibilities, and, from a technological point of view, this is where we hope to find the most interesting results.

MATERIALS AND METHODS

D-(+)-trehalose dihydrate (Pfanstiehl Laboratories, 98.9%) and sodium chloride (Aldrich Chemical Company, 99+% ACS reagent) were used without any further purification. Milli-Q water (10^{18} MW·cm) was used for all experimental work. All solutions were prepared gravimetrically on an analytical microbalance. Most solutions required heating and mixing to dissolve the solute(s). Solutions were heated in sealed glass vials in a constant temperature bath.

Amorphous trehalose was prepared by freeze drying a 10wt% solution of trehalose using a FTS Systems tray dryer coupled with a Dura-Dry MP condenser module. The trehalose solution was cooled to −45°C under vacuum (10^{-2} mbar) and held for 72 hours. The temperature was increased to 0°C over 4 days. The sample was then dried in a vacuum oven at room temperature for 2 days, followed by drying at 70°C for 2 days to remove residual water. All subsequent handling of the samples was done in a dry nitrogen atmosphere. The water content

of the amorphous samples was determined to be less than 0.2wt%, as measured by Karl Fischer titration.

Differential Scanning Calorimetry

A Netzsch DSC-200 differential scanning calorimeter was used for calorimetric measurements. An 11-point calibration of both temperature and enthalpy was done for each set of conditions. Approximately 20 mg of each solution was weighed in a Netzsch TG 209 thermogravimetric analyzer at 20°C, and sealed in a 40 μl aluminum pan with a crimping press. An empty aluminum pan, identical to that used for the sample, was used as the reference. The sample was immediately quenched by plunging the sealed pan directly into liquid nitrogen. This method of quenching restricted our experiments to trehalose concentrations above 60wt%.

All DSC data were collected in heating mode. Nitrogen vapor, produced by heating liquid nitrogen in a dewar, was used to pre-cool the sample cell to temperatures about 40°C below the expected T_g. The sample pan was then quickly transferred from the liquid nitrogen quench bath to the sample cell. The sample was thermally equilibrated for 5 minutes before beginning the experiment at scan rates of 5 and 10°C/min. The faster scan rate was used to increase sensitivity to the glass transition. The sample cell was continually purged with dry N_2 gas (99.9995% pure) at 25 ml/min. Nitrogen from the same source was also used as a protective gas to prevent condensation of water on the DSC cell (300 ml/min). Sample preparation and experimental conditions were chosen according to ASTM standard test method E 1356-91.

The glass transition was determined by constructing tangents to the DSC curve baselines before and after the glass transition. The intersection of these tangents to the tangent at the inflection point gives the extrapolated onset and endpoint temperatures. As is customary, the midpoint of these temperatures is reported as the glass transition temperature.

Dynamic Mechanical Analysis

Dynamic mechanical analysis of the frozen samples was performed with a Perkin-Elmer DMA 7e apparatus using the parallel-plate probe. The DMA analyzer measures the amplitude of the oscillation at a given frequency and the phase lag (δ) of the response with respect to the applied force. In our experiments, normal forces were adjusted dynamically to maintain oscillations of 1–2 μm in amplitude. The DMA was operated in the temperature scan mode at scan rates of 5 and 10°C/min.

For a DMA run, the entire apparatus (probe and stage) was cooled to about 40°C below the expected glass transition temperature. A drop of sample at room temperature was placed in a 6 mm diameter aluminum pan and quenched in a bath of liquid nitrogen. The typical sample thickness was between 1 and 3 mm. The glass transition temperature was inferred directly from the probe position curve. Tangents to the linear sections of this curve were constructed both before and after the glass transition. The intersection of these lines is defined as the softening point, T_s. The relationship between the softening point and T_g has been discussed by Shalaev and Franks (27). They suggest that the sample will retain its solid-like behavior at temperatures slightly above T_g and argue that viscous flow in real time is not measurable by DMA until temperatures somewhat above the T_g measured by DSC. The mechanical deformation at such temperatures will, of course, depend upon the parameters of the experiment such as the scan rate, the oscillation frequency, and the applied force.

X-Ray Diffractometry

A Siemens diffractometer with a Cu-Kα source and a HI-STAR area detector was used for the x-ray diffraction experiments. Samples were packed and sealed into 1 mm quartz capillaries in a dry nitrogen atmosphere. Rotation scans at $2\Theta = 0°$ were performed for 30 minutes and background scans were subtracted. For experiments at elevated temperatures (up to 110°C), an FTS Systems Air Jet Crystal Cooler controlled the sample temperature.

Viscometry

Viscosities of trehalose solutions were measured using a Bohlin CVO controlled stress rheometer with a parallel plate measuring system. The minimum temperature allowed by the cooling system was −25°C. The gap between plates was set between 0.3 and 1.0 mm, while the shear stress varied from 3 to 500 Pa. The shear stress was adjusted through trial and error to give a sufficiently high strain rate (1–300 s^{-1}) without crystallizing either trehalose or ice from the sample. Several measurements were performed at intervals of 20–30 seconds.

Solid-Liquid Phase Diagram

The solubility of trehalose in water was determined by measuring the concentration of trehalose in the supernatant aqueous phase of a saturated trehalose/water mixture. The mixture was vigorously stirred at 1000 rpm for eight hours in a 200 ml test tube immersed in a constant temperature bath. It was then sealed to prevent evaporation and allowed to settle until a clear supernatant phase was obtained. The concentration of trehalose was measured using an Abbe refractometer. The equilibrium condition was determined by periodically measuring the concentration of the aqueous phase until a constant value (within ±0.05wt%) was obtained. The mixture was stirred and allowed to settle before each measurement. Experiments were performed in triplicate. The stability of the temperature bath was ±0.1°C. The effective resolution of the Abbe refractometer was ±0.1wt%.

The freezing point depression of the binary trehalose water mixture was measured using a method similar to that described by Scatchard *et al.* (30). Two closely matched 200 ml vacuum dewars were used for the solution and the ice-water reference bath. The solution consisted of finely chopped ice in equilibrium with aqueous trehalose. The ice was prepared from Milli-Q water, and then chopped in a household blender. Both baths were continually stirred. The temperature was measured with a pair of thermistor probes and a resistance bridge. The uncertainty in the temperature measurement was ±0.03°C. The concentration of the aqueous solution was measured using an Abbe refractometer.

Heat of Solution Calorimetry

The heats of solution of amorphous trehalose and trehalose dihydrate were measured using a Thermometrics 2225 High-

Precision Solution Calorimeter in a Hart 7037 constant temperature bath. Temperature stability of the bath was better than 0.1 mK over the duration of the experiment. Approximately 0.1 g of sample were placed into a thin-walled glass ampoule and sealed with a silicone stopper and beeswax. The sealed ampoule was immersed in 100 ml of Milli-Q water inside the glass reaction vessel. The contents of the cell were stirred at 400 rpm. Five electrical calibrations were performed both before and after breaking each ampoule.

Specific Volume

The densities of trehalose solutions with concentrations ranging from 18 to 68.5wt% were measured using an Anton-Paar DMA 40 vibrating tube densimeter. These measurements were made in the temperature range from −15°C to 20°C. The instrument was calibrated using diethyl ether and methanol, whose densities below 0°C are known (31,32). Most of the solutions were supersaturated due to the low temperatures. This led to complications with crystallization of ice. In most cases, crystallization could be avoided by judiciously choosing experimental conditions. Solutions were prepared by heating gently to temperatures just above the equilibrium solubility temperature. Approximately 2 ml of solution were then injected into the densimeter, which was pre-cooled to the measurement temperature. The solution was allowed to cool to the measurement temperature before turning on the densimeter. This prevented the oscillations of the tube from inducing nucleation. The glass tube allowed for a visual check for any obvious signs of crystallization. Measurements were done in triplicate. The uncertainties in the temperature and density measurements are ±0.02°C and ±0.0005 g/cm^3, respectively.

RESULTS AND DISCUSSION

Solid-Liquid Phase Diagram

Figure 1 shows the equilibrium phase diagram of the trehalose/water system. These data cover the concentration range from 0 to 80wt% trehalose. The solubility of trehalose dihydrate in water is reported in Table I. As can be seen in Fig. 1, these values are significantly lower than previously reported for this saccharide.

The discrepancies between our data and the solubility results above 0°C reported by Nicolajsen and Hvidt (26) could be explained if we bear in mind the slow precipitation of the solid from the supersaturated solution, especially for high-viscosity systems. The supercooling of saccharide solutions is a well-known phenomenon (33). An experiment that uses the method of cooling a supersaturated solution and waiting for precipitation to occur is prone to kinetic limitations; the temperature at which the solute precipitates from a mixture of known composition can be underestimated, even with the use of techniques that promote nucleation and crystal growth. The agreement between the differential scanning calorimeter (9) and short-term (26) experiments is surprising, especially considering the different experimental techniques that were used, but it could be a sole consequence of the similarity of the time scales assessed by the two experiments.

Another plausible argument for the discrepancy between our results and those of others involves the formation of crystalline hydrates. Many low molecular weight saccharides exhibit multiple crystalline hydrate forms (34–36). It is possible that, during short term experiments, only a metastable state is attained between the solution and a crystalline hydrate. In the long term experiments, a different, thermodynamically stable solid species could be achieved, thereby shifting the solubility curves.

It should be noted that *some* of the discrepancy between our solubility measurements and those of others may be attributed to

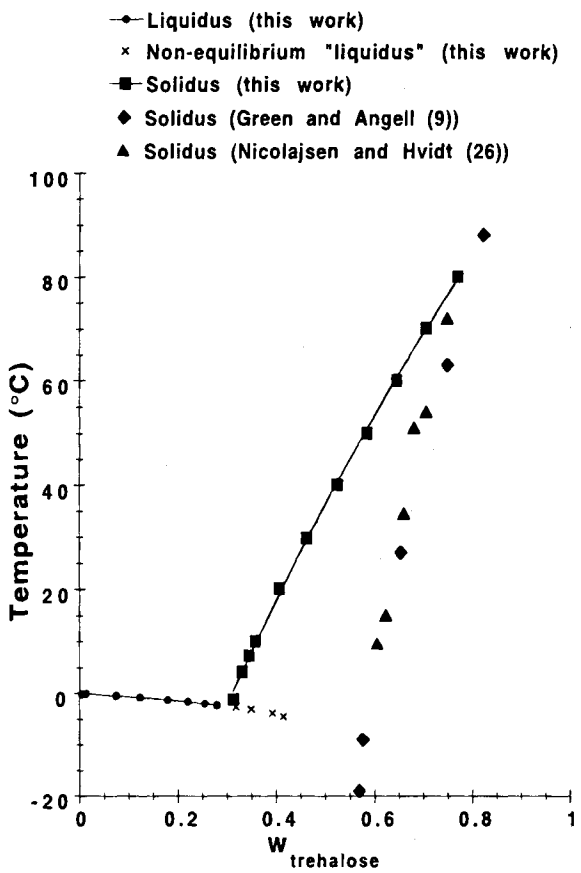

Fig. 1. Equilibrium phase diagram of trehalose as measured by other groups and in our laboratory. The solutions for the data points noted as "non-equilibrium liquidus" appeared cloudy during measurements and are thought to be beyond the equilibrium eutectic point. Data of Green and Angell (9) and Nicolajsen and Hvidt (26) are provided for comparison. The concentration unit is weight fraction trehalose.

Table I. Solubility of Trehalose in Water

Temperature (°C)	wt% Trehalose
−1.20	31.2
4.11	33.1
7.27	34.5
10.0	35.8
20.2	40.6
29.8	46.2
40.1	52.4
49.9	58.4
60.1	64.4
70.1	70.4
80.0	76.9

sample purity. Small amounts of ionic impurities should, in principle, reduce the solubility of the trehalose by a "salting out" effect. The trehalose purity used in these studies was 98.9%; the purity of the trehalose used by other workers (9,26) was not reported.

The ability of saccharide solutions to supercool is one of the properties that makes them useful cryoprotectants. This is demonstrated by experiments (37) in which 60wt% solutions of fructose, mannose, ethyl mannoside, and ethyl glucoside remained pourable liquids (completely free of ice and solute crystals) during more than 4 years of storage at −18°C, which is well below their equilibrium freezing points. Regardless of such kinetic limitations, however, precise knowledge of solubility is essential for design of suitable formulations and processing conditions.

The liquidus curve includes some points in which a "milky" solution was observed during experiments. These observations confirm that the concentrations of the aqueous phase were greater than the eutectic. The intersection of the liquidus and solidus curves defines the equilibrium eutectic point, which lies at −2.5°C and a concentration of 29.8wt% trehalose. Our measurements clearly show a eutectic temperature more than 15°C greater than that measured by Green and Angell (9), −18.8°C, but only slightly above the value reported by Nicolajsen and Hvidt (26), −4.4°C.

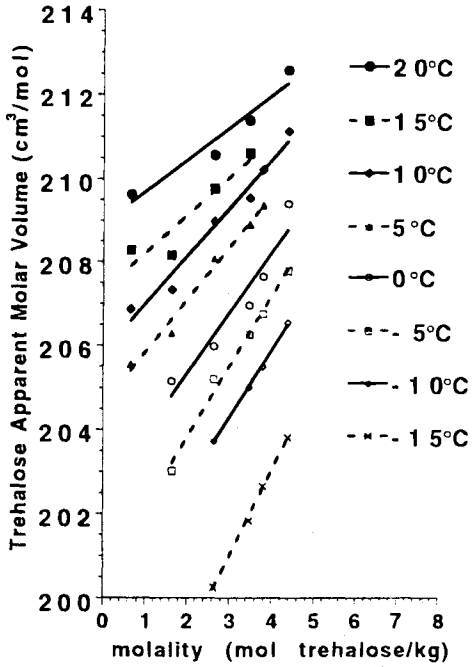

Fig. 2. Apparent partial molar volume of trehalose at several temperatures.

Volumetric Properties of Trehalose Solutions

It is well-known (22) that trehalose has the smallest apparent partial molar volume of the common disaccharides: trehalose, maltose, lactose, cellobiose, and sucrose. The apparent partial molar volume, V_ϕ(cm³/mol), of trehalose in aqueous solution was calculated from the measured density by the relation:

$$V_\phi(T) = \frac{1000(\rho_w - \rho_d)}{m\rho_w\rho_d} + \frac{M}{\rho_d} \quad (1)$$

where ρ_w(T) and ρ_d(T) are the densities of water and solution (g/cm³), respectively, m is the molality of the solution and M is the molecular weight of trehalose (342.3 g/mol). Figure 2 shows the results as a function of concentration at temperatures between −15°C and 20°C. These results indicate that V_ϕ is a linear function of trehalose concentration, as expected for a non-electrolyte solute. Also note that the rate of change of apparent partial molar volume increases as the temperature is lowered.

The values of partial molar volume at infinite dilution, V^∞, were obtained by extrapolation of the linear regressions in Fig. 2; results are given in Table II. For comparison, we provide data from other authors. The agreement is fairly good. Note that our results involved large extrapolations to zero-trehalose concentration, and should therefore be regarded with caution. However, some general conclusions can be deduced. At 20°C, the molar volume of crystalline (anhydrous) trehalose dihydrate is 216.6 cm³/mol (38) and that of amorphous trehalose is 222.3 ± 2.9 ml/mol (39). The results in Table II indicate that there is a slight volume contraction of trehalose when it dissolves in water. The partial molar volume at infinite dilution, which is a measure of hydration (solute-solvent interactions), increases with temperature.

We conclude that as temperature decreases from 20°C to −15°C, V^∞ decreases by about 14 cm³/mol, which is equivalent to almost one mole of water per mole of trehalose. At this point, it is not possible to ascertain whether this volume reduction corresponds to a folding of the disaccharide or to stronger hydration. Molecular dynamics studies of trehalose in water (11) concluded that one trehalose molecule interacts directly with at least ten water molecules. That work suggested that an internal hydrogen bond can be formed between OH(6) and OH(2) of the different pyranose rings due to partial folding of these rings along the glycosidic linkage. We can speculate that this folding increases at low temperatures, leading to the observed volumetric effect.

Table II. Partial Molar Volume of Trehalose at Infinite Dilution at Several Temperatures

Reference	Temperature (°C)	$V^\infty\left(\frac{cm^3}{mol}\right)$
(18)	25	209.77
(22)	25	208.0
(25)	25	206.9
this work	20	208.9
this work	15	207.3
this work	10	205.8
this work	5	204.6
this work	0	202.4
this work	−5	200.4
this work	−10	199.5
this work	−15	194.8

Note: Results of other authors are provided for comparison.

Glass Transition Temperature

Figure 3 shows the glass transition temperature data for the trehalose/water system. The data were measured using both DSC and DMA. Note that the DMA method consistently gives a T_g that is a few degrees above that obtained by DSC. As mentioned earlier, this is due to the manner in which the glass transition temperature is assigned when analyzing DMA data. Using this method, the probe position curve has a marked decrease at temperatures below the extrapolated onset temperature. That is, the sample probe has significantly penetrated the sample before the extrapolated onset temperature is reached. A typical probe penetration at the extrapolated onset temperature is 0.2 mm, while the minimum measurable probe displacement is about 0.001 mm. For the solutions studied, the typical difference in temperature between the extrapolated onset and the temperature of first deviation of the probe tip from its initial position is about 6°C. This corresponds to a decrease in viscosity of nearly two orders of magnitude, as calculated from the WLF equation (see below). This could explain the difference between the glass transition temperatures obtained from DSC and DMA measurements. Despite the difference, however, the dynamic mechanical analysis provides an unequivocal validation of the results of DSC, which can sometimes be difficult to interpret.

Published glass transition temperature measurements of amorphous trehalose exhibit marked differences. This variation is probably due to the presence of residual water in the samples. Water is an excellent plasticizer of amorphous sugars. Trace amounts of water increase the molecular mobility in the system, thereby reducing the glass transition temperature. We have measured the T_g of amorphous trehalose to be 114.9°C. The possibility that this is a (enthalpic relaxation) collapse event and not a true glass transition, as suggested by the work of Shalaev and Franks (27), has been discounted through the use of repeated scans. That is, the sample was heated through its reported glass transition, cooled to 30°C below this temperature, and then reheated. The value reported is for the second scan. The amorphous character of this sample has been verified with x-ray diffraction at a temperature (105°C) slightly below the measured T_g. In Fig. 4, the powder patterns of trehalose dihydrate and anhydrous trehalose are provided for comparison.

Figure 5 shows the glass transition temperatures of trehalose/sodium chloride/water mixtures. Three concentrations of trehalose were studied: 7.5, 10, and 15 mole percent. Various amounts of sodium chloride were added to yield solutions with up to 10 mol% NaCl. The data show that NaCl is relatively ineffective at raising T_g. Its effect on the T_g of each trehalose solution was similar; a concentration of 10 mol% NaCl raised the T_g by about 8°C in each case. Note that the physiological concentration is less than 0.2 mol% NaCl. Interestingly, even though the addition of NaCl has relatively minor effects on the glass transition, it profoundly affects the crystallization kinetics of ice (Fig. 6). The 7.5 mol% trehalose solution prepared without NaCl crystallized almost immediately following its glass transition. The addition of even small amounts of NaCl completely suppressed crystallization; a ternary solution with 5 mol% NaCl did not crystallize over the time scale of our experiment.

We have recently proposed a simple model for predicting T_g (40) (Appendix A). Its usefulness resides in that it requires no adjustable parameters and is based on volumetric data that can be readily measured in the laboratory. This free-volume model relates the glass transition temperature to the percolation

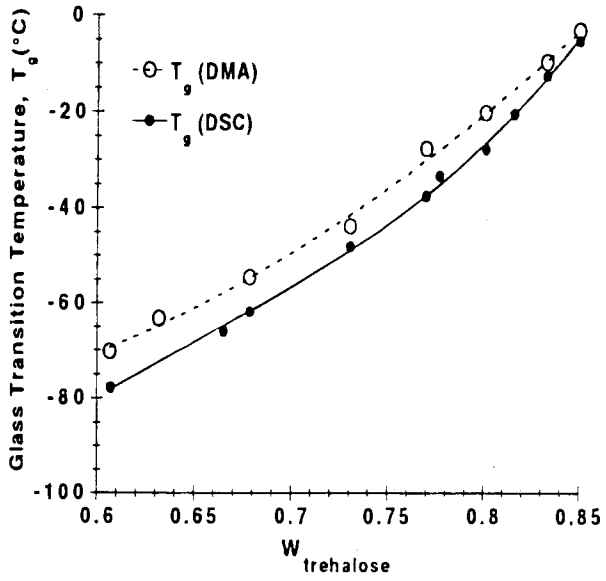

Fig. 3. Glass transition temperature of aqueous trehalose solutions. All DSC and DMA scans generated at 5°C/min heating rate. The uncertainty in the DSC temperature measurement is ±1°C, while that of the DMA is ±2.5°C. The concentration unit is weight fraction trehalose.

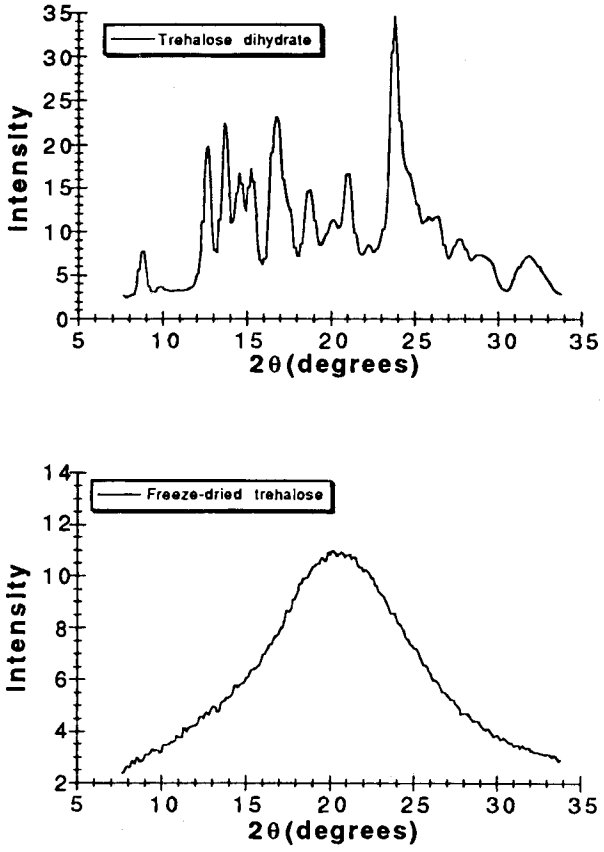

Fig. 4. X-ray powder patterns for trehalose dihydrate and amorphous trehalose. Powder pattern for amorphous trehalose was taken at 105°C. Powder pattern for trehalose dihydrate was taken at 25°C. The intensity scales are not normalized.

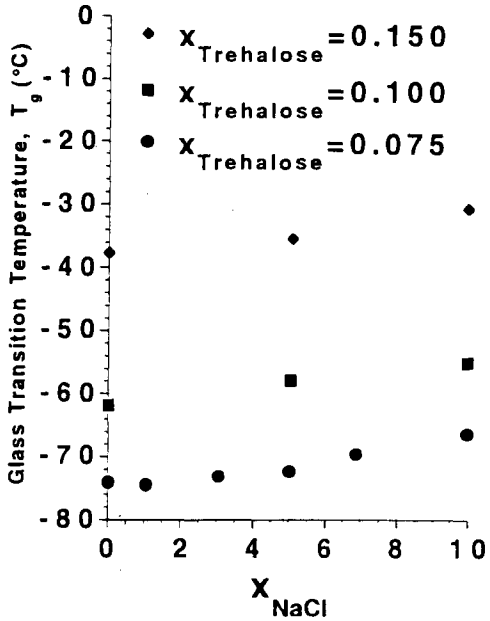

Fig. 5. Glass transition temperature for several trehalose/sodium chloride/water solutions. All DSC scans were generated at a 10°C/min heating rate. The uncertainty in the temperature measurement is represented by the size of the symbols. The concentration unit is mole fraction sodium chloride.

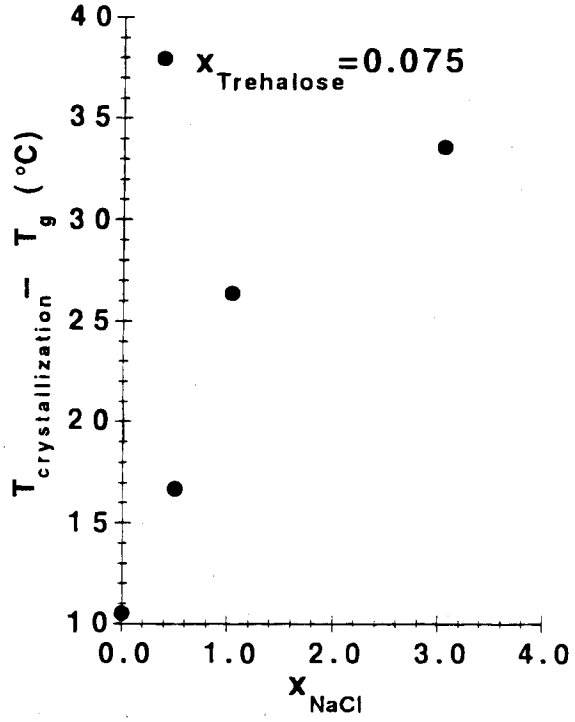

Fig. 6. The effect of the addition of sodium chloride to aqueous trehalose solutions on the crystallization temperature of ice. The concentration unit is mole fraction sodium chloride.

threshold of a 3-dimensional system. Percolation readily occurs at temperatures far above T_g. That is, there is sufficient free volume for translational molecular motion throughout the system. However, as the temperature is lowered, the free volume of the system decreases, thereby restricting molecular motion. At the percolation threshold, which corresponds to a free volume fraction of 0.16, the long-range continuity of the system is broken, and motion is arrested. The temperature at which this free volume "catastrophe" occurs is determined by extrapolating volumetric data from several temperatures above the glass transition. The free volume of the system is extrapolated to lower temperatures until the percolation threshold is reached. Although the concept of the percolation threshold is appealing, we have found that the model predictions are relatively insensitive to the particular value of that threshold. For simplicity, the predictions of the glass transition temperature in this work have been obtained by neglecting the term containing excess quantities in Eqs. A7 and A8. For the trehalose solutions studied here, the entire contribution of the last term of Eq. A8 is about two orders of magnitude smaller than that of all other terms.

Couchman and Karasz (41) have presented a model that uses classical thermodynamics to predict the compositional dependence of T_g (Appendix B). The model requires calorimetric data for the pure systems, namely the change in the heat capacity (C_p) at T_g (and the T_g) of each component.

Table III shows both experimental data and predictions from our model for several aqueous trehalose systems. Agreement of our model with available experimental data for the binary and ternary systems is satisfactory. The single trehalose/NaCl/H_2O system studied and the 60wt% binary trehalose solution both contain about 7.5 mol% trehalose. A comparison of the model predictions for these two mixtures shows that our model is qualitatively correct; the addition of sodium chloride slightly raises T_g. The model prediction for the ternary system assumes that the T_g of NaCl is 1000 K. The model is relatively insensitive to this choice since the NaCl mole fraction is small.

Table III also shows the predictions of the "Couchman-Karasz model" using ΔC_p = 35 JK^{-1} mol^{-1} (42) and T_g = 136 K for pure water. We measured ΔC_p = 215 ± 18 J/K^{-1} mol^{-1} at T_g = 388 K for amorphous trehalose. Table III shows that the predictions of this model are remarkably accurate over the entire concentration range studied.

Note, however, that the heat capacity difference between the supercooled liquid and glassy "states" of pure water at its T_g has been a matter of much debate (43). Based on heat capacity data for supercooled liquid water and the ΔC_p result reported by Sugisaki *et al.*, Johari (44) used thermodynamic arguments to postulate that there is no continuity of state between amorphous solid water (ASW) and supercooled liquid water. Recently, Hallbrucker *et al.* (45) have measured ΔC_p for the glass to liquid transition of pure water at T_g to be 1.6 ± 0.1 JK^{-1} mol^{-1}. This value is considerably lower than that previously reported (42) or estimated (46,47) by other authors. Hallbrucker *et al.* (48) have used this lower ΔC_p to construct thermodynamic pathways connecting the ASW and supercooled liquid water states, thereby eliminating the thermodynamic paradox. More recently, Speedy *et al.* have measured the evaporation rates of ASW and ice near 150 K to develop an estimate for the residual entropy of the glass (49). That result showed that supercooled water and ASW satisfy bounds imposed by thermodynamic consistency, implying that a continuity of states

Table III. Predictions of the T_g of Aqueous Trehalose Solutions Using the Models of Kolker *et al.*, Couchman and Karasz, and Soesanto and Williams (Eqs. 2 and 3)

wt% Trehalose/NaCl/H_2O	T_g (°C) model of Kolker *et al.*	T_g (°C) model of Couchman-Karasz	T_g (°C) predicted using Eqs. 2 and 3	T_g (°C) measured
57.9/6.6/35.5	−84		−78	−73
60.0/0.0/40.0	−90	−81		−80
65.0/0.0/35.0	−72	−70	−74	−68
68.5/0.0/31.5	−70	−62		−60
72.4/0.0/27.6	−58	−52	−61	−51
80.0/0.0/20.0	−29	−26		−27
83.0/0.0/17.0	−15	−13		−15

Note: Experimental results (DSC scans at 5°C/min heating rate) are provided for comparison. Measurements and predictions are rounded to the nearest °C.

is possible. The T_g predictions of the Couchman-Karasz model are very inaccurate when using the lower value of ΔC_p. The assumption in the derivation of Eq. B5 that ΔC_p is independent of temperature and the anomalous C_p behavior for supercooled liquid water are likely causes for the failure of their model in predicting T_g for this aqueous system.

Heat of Solution

We measured the heat of solution at 25°C of amorphous trehalose to be −25.3 ± 0.1 kJ/mol (final molality, m = 2.9 · 10^{-3} mol trehalose/kg H_2O). The heat of solution of trehalose dihydrate at 25°C was measured to be +20.7 ± 0.2 kJ/mol (m = 2.0 · 10^{-3} mol trehalose dihydrate/kg H_2O). This is in good agreement with the value reported by Jasra and Ahluwalia (18), +20.3 ± 0.08 kJ/mol, which was determined from a trehalose · 1.86 H_2O sample. We deduce from these results that the formation of the dihydrate from the amorphous solid is strongly exothermic. Furthermore, the dissolution rate of the amorphous solid is noticeably faster than that of the crystal.

Viscosity

We have determined the dynamic viscosity of four aqueous trehalose solutions. The results are summarized in Table IV. The empirical equation proposed by Williams, Landel, and Ferry (50) is often used to describe the temperature dependence of viscosity:

$$\log \frac{\eta}{\eta_g} = -\frac{C_1(T - T_g)}{C_2 + (T - T_g)} \tag{2}$$

The "WLF equation" is intended for use from T_g to T_g + 100 K, and for solution viscosities greater than 10 Pa·s. For well-behaved polymers, C_1 and C_2 are "universal constants," which take on values of 17.44 and 51.6, respectively. A typical value of η_g, which denotes the viscosity of the glass, is $10^{13.6}$ Pa·s. Although Eq. 2 has been widely used with the above values of C_1, C_2 and η_g, it has also been recognized that C_2 is far from universal and that a variety of molecular liquids have a viscosity as low as 10^9 Pa·s at T_g (51).

In the past, the WLF relation has been used successfully to correlate the viscosity of concentrated fructose/sucrose blends with the glass transition temperature (52). The T_g predicted by the WLF equation depends strongly upon the value of η_g; the commonly used value, $10^{13.6}$ Pa·s, is conveniently based on a relaxation time of one day (53). For saccharide solutions, Soesanto and Williams (52) have proposed a relation to predict η_g as a function of sugar concentration (x) based on the molar volume of the solution, $V(x)$. It is given by the expression:

$$\eta_g(x) = Ae^{kV(x)} \tag{3}$$

where the values A = 3.99 · 10^{10} Pa·s and k = 38.74 mol/l are based on data for the melts of a fructose/sucrose mixture and glucose.

Table IV. Dynamic Viscosity of Several Concentrated Aqueous Trehalose Solutions from −25°C to +20°C

39.2 wt% Trehalose		65.0 wt% Trehalose		72.5 wt% Trehalose		57.9/6.6/35.5 wt% Trehalose/NaCl/H_2O	
Temperature (°C)	Viscosity (Pa·s)*100	Temperature (°C)	Viscosity (Pa·s)	Temperature (°C)	Viscosity (Pa·s)	Temperature (°C)	Viscosity (Pa·s)
20	1.16	5.0	1.04	0.0	34.0	−13	3.50
15	1.18	−5.0	3.03	−5.0	62.0	−15	4.58
10	2.22	−10	4.58	−10	78.0	−17	5.80
5.0	2.75	−13	7.10	−15	192	−20	8.70
0.0	3.50	−17	12.1	−20	417		
−5.0	4.53	−20	20.0	−23	680		
−10	6.20	−24	39.0				
−15	9.00						

Note: The uncertainty of a viscosity measurement is approximately ±5%.

The WLF equation, in conjunction with Eq. 3, can then be used to predict T_g based on readily available volumetric and viscometric data at 20°C. Table III shows the predicted T_g and the measured value for several trehalose solutions. The T_g predictions using this method are reasonable. The agreement is surprising since the commonly accepted values for the constants C_1 and C_2 fail to fit our $\eta(T)$ data for any chosen values of T_g and η_g.

The scaled Arrhenius representation of viscosity data is commonly used as a method to classify liquids as either fragile or strong. Using this method, the reduced viscosity of the solution is shown in Fig. 7 as a function of the reduced temperature. A fragile liquid will form a glass that, when heated above its T_g, exhibits a large decrease in viscosity with a small increase in temperature. On the other hand, a strong liquid forms a glass that resists thermal degradation. Our results only cover a small region of the scaled Arrhenius representation of the viscosities, but they clearly indicate that the behavior of the trehalose/water concentrated solution is similar to that of other fragile liquids, such as sucrose. For comparison, data for an aqueous sucrose solution (54) and the strong glass-former SiO_2 (55) are also given in Fig. 7.

Supplemented Phase Diagram

Figure 8 shows the so-called supplemented phase diagram for the trehalose/water system. This figure not only includes equilibrium data, but also the glass transition curve and the liquidus curve extrapolated beyond the eutectic point. The supplemented phase diagram is useful for illustrating the concentration regime in which a system passes from thermodynamic to kinetic control. That is, there is a specific trehalose concentration, C_g', beyond which water from the mixture cannot be further crystallized on experimental time scales. For a mixture, C_g' is identified as the point of intersection of the glass transition curve and the extrapolation of the equilibrium freezing point depression curve; T_g' is the glass transition temperature of this mixture. Constructing the curves using our data gives C_g' and T_g' equal to 81.2wt% and −22.2°C, respectively. These values are significantly different from those reported in the literature (Table V).

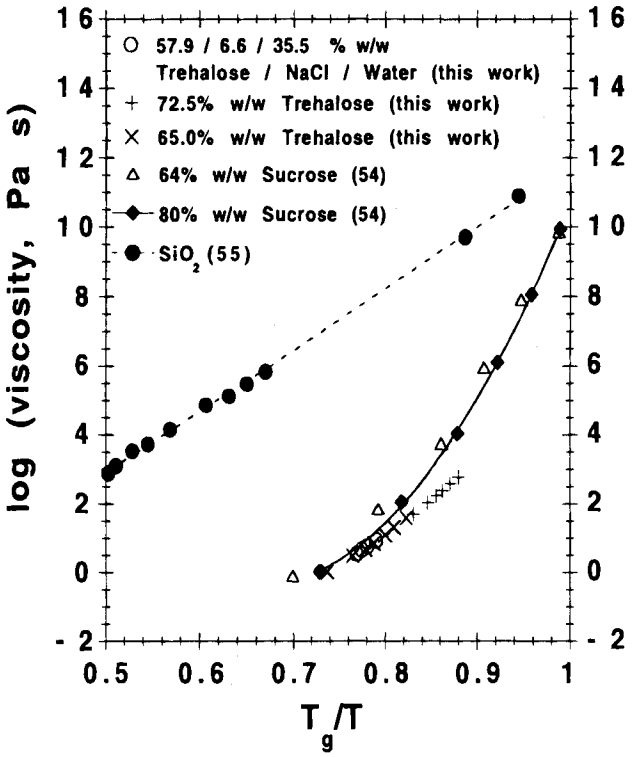

Fig. 7. Scaled Arrhenius representation of viscosity data for trehalose/water solutions. Aqueous sucrose (54) data and SiO_2 (55) data are provided for comparison.

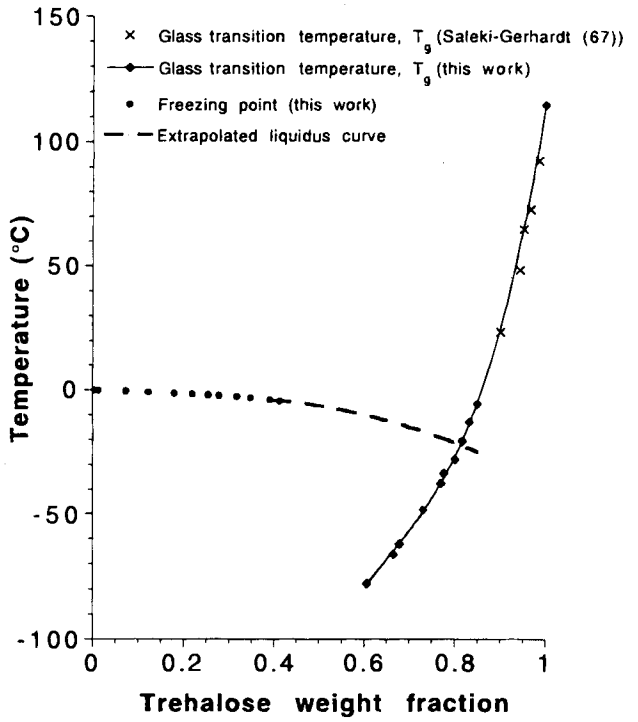

Fig. 8. Supplemented phase diagram for the trehalose/water system. The liquidus curve is extrapolated to the T_g curve to illustrate the point of maximum freeze concentration, C_g', T_g'. T_g data of Saleki-Gerhardt (67) are provided for completeness.

Table V. Maximum Freeze Concentration (C_g') and Its Glass Transition Temperature (T_g') as Reported by Various Authors

Reference	C_g' (wt% Trehalose)	T_g' (°C)	T_g (°C) (this work)
(65)	Not reported	−31.8	
(19)	83.3[a]	−29.5	−12.8
(28)	81.6[b]	−35	−20.6
(26)	Not reported	−30	
(57)	70.5[c]	Not reported	−57.4
this work	81.2	−22.2	−22.2

Note: All data are from DSC scans at 5°C/min heating rate, with the T_g' taken as the midpoint of the extrapolated onset and endpoint temperatures.

[a] Unfrozen water calculation based upon ice melting endotherm of a single solution.

[b] Unfrozen water calculated using Gordon-Taylor expression (66).

[c] Unfrozen water calculation based upon extrapolation of results from a series of solutions.

For aqueous saccharide systems, the parameters C_g' and T_g' are particularly meaningful since crystallization of the saccharide does not occur on experimental time scales (33). Instead, ice continues to precipitate as the aqueous mixture is cooled; the composition of the remaining solution follows the liquidus curve beyond the equilibrium eutectic point. At some concentration, the liquid remaining within the ice matrix becomes kinetically inhibited from freezing, and, upon further cooling, undergoes a glass transition; C_g' is the concentration of the freeze-concentrated solution and its glass transition temperature is T_g'. The quantity C_g' is important since all freezing and drying processes must, in principle, pass through this point during either cooling, drying, warming or hydration.

The quantity T_g' has important implications for freeze drying (lyophilization) processes. Lyophilization is usually performed below T_g' to avoid a phenomenon known as collapse. At a temperature near or above T_g', the sample flows during processing, thereby leading to a loss of porosity. Eventual collapse of the sample results in low rates of mass transfer of residual water out of the sample and an inferior product. Avoiding collapse is important for maintaining product quality during lyophilization.

The differences between our C_g' and T_g' values and those reported probably result from the method of measurement. Our result is based on independent measurements of liquidus and T_g curves; other methods rely on conditions in which both ice formation and vitrification occur. Those techniques may suffer from kinetic limitations. The various methods have been previously reviewed; we briefly summarize them here. Some workers (56,57) have determined C_g' by extrapolation. Using this method, several solutions covering a wide range of different initial concentrations are prepared and then subjected to the same cooling program. The enthalpy of the ice melting endotherm is then measured for each solution. The enthalpy of this peak per unit mass of solute is plotted against the mass ratio of water to solute in the original solution. Extrapolation of this curve to zero-ice-melting-peak corresponds to the C_g' value. This method assumes that the endotherm is solely due to the melting of ice; it neglects other possible thermal events such as eutectic melting. Slade and Levine (37) have criticized this method on the basis that the series of prepared solutions has a wide range of characteristic time scales, and that heating and cooling all solutions at the same rate invalidates the method.

Slade and Levine (19) have slowly cooled a dilute trehalose solution (10wt%) to maximize the amount of precipitated ice. The enthalpy of the ice-melting endotherm is measured using DSC. The magnitude of this endotherm, along with the enthalpy of fusion of pure water, is then used to calculate the quantity of ice frozen. The trehalose concentration in the aqueous (continuous) phase can then be calculated. Strictly speaking, calculations using this method must account for the temperature and solution composition dependence of the molar latent heat of fusion.

Our quenching method could provide yet another explanation of the differences between our T_g' value and reported values. We expect that the glass transition temperature of our samples that were quenched in liquid nitrogen will be higher than that of samples prepared by a slow cooling method.

In the highly concentrated region above C_g', T_g exhibits a marked dependence on the concentration of water. A change in trehalose concentration of ± 1.0 wt% can change T_g by ± 5°C. To verify our results for C_g' and T_g', we prepared solutions of the same concentration as the C_g' given in Table V. The solutions were quench cooled in liquid nitrogen and then the T_g was determined with DSC scans at 5°C/min. We found that while these T_g values were consistent with our supplemented phase diagram, they were significantly different from those reported in the literature.

Regardless of the method used, the point defined by the C_g' and T_g' values should lie on the curve of glass transition temperature versus concentration (Figs. 3, 8). In this work, the data for the T_g curve were measured by quenching homogeneous solutions. It is assumed that, for the concentrations studied, quenching was sufficiently fast to prevent phase separation. The reported T_g' values vary from author to author, but are generally around -30°C (Table V). This is the T_g of a 79wt% trehalose solution, as interpolated from our T_g results.

CONCLUSIONS

The scarcity of fundamental data on the trehalose/water system, particularly in the concentrated regime, has prompted us to perform some of these much needed measurements. The equilibrium liquidus and solidus curves were measured. We determined that the solubility of trehalose in water is significantly lower than previously reported (9,26). We attribute this difference to the substantially longer times employed to attain equilibrium in our measurements. We also speculate that the presence of a metastable crystalline (trehalose) hydrate may explain the solubility results of short-term experiments. Glass transition temperatures for these solutions were measured using two independent methods. The glass transition temperature of amorphous trehalose was found to be greater than that reported in previous studies (9,58). We believe that this is due to residual moisture content in the samples employed by previous authors. Enthalpy of solution for both amorphous and crystalline trehalose was measured. We suspect that there is a correlation between these quantities and the protective ability of the saccharide. The heat of solution of a compound in water provides a measure of its ability to form hydrogen bonds. Thus, for protective agents, the water replacement hypothesis should be consistent with large negative heats of solution. We are currently investigating this possibility by measuring the enthalpy of solution of a variety of amorphous saccharides. These data should provide insight into trehalose's effectiveness as a protective agent.

Volumetric and viscometric properties were measured as a function of temperature for several concentrations of trehalose. Studies that attempt to predict the glass transition temperature of such mixtures should benefit, since many theories of the glass transition are based either on free volume or an isoviscosity state. We have presented a previously unpublished model that predicts the glass transition temperature based solely on volumetric data. The predictions of our model are in good agreement with experiment.

It was also shown that, with regard to the general classification scheme of strong/fragile glass-forming liquids, trehalose solutions are fragile liquids. This behavior is consistent with that of other concentrated saccharide solutions.

The kinetic properties of a model ternary solution, trehalose/sodium chloride/water, were studied. The effect of the electrolyte component on both the glass transition tempera-

ture and the recrystallization temperature was investigated. Low concentrations (<5 wt%) of sodium chloride increased the glass transition temperature only slightly. A recent theory (59) predicts that dissociated charged species dramatically raise T_g. We have been unable to corroborate this claim with aqueous solutions (60). In future work, we will investigate the influence of various electrolytes and their degree of dissociation on the glass transition temperature of aqueous trehalose solutions.

Although the addition of sodium chloride only slightly increased T_g, the temperature at which ice recrystallized from the mixture increased significantly. The presence of an electrolyte, therefore, has significant implications regarding processing and formulation conditions (61). We are currently investigating the effects of various electrolytes on crystallization kinetics.

APPENDIX A

The purpose of this addendum is to present a simple general relation between the glass transition temperature of a non-ideal binary or multicomponent solution and its composition. Such a relation would provide general guidelines as to which types of glass formers are likely to yield the desired range of T_g for mixtures.

The liquid to glass transition can be qualitatively described as follows (62). One of the main differences between a liquid and an amorphous solid is that the liquid has sufficient free volume, V_f, to permit frequent diffusive motion of its molecules. This gives rise to the so-called "fluidity" of a liquid. It is important to emphasize here that the free volume must be continuous throughout the system to permit the macroscopic fluidity of the whole body. In other words, geometrically, the free volume of the liquid can be interpreted as a continuous network of "lakes and channels". With decreasing temperature, the total volume V of the liquid decreases and the free volume V_f also decreases; at some temperature, the free volume is reduced to a critical level below which the continuous network of "lakes and channels" disintegrates. Below this temperature, there is insufficient room for molecular mobility throughout the whole system and, consequently, for the macroscopic manifestation of fluidity. With regard to this concept of a liquid, the temperature at which such a disintegration occurs corresponds to the glass transition.

This qualitative picture of the glass transition can be conveniently treated in a somewhat quantitative manner by applying one of the numerical results of percolation theory; namely, that there is a constant critical volume fraction at which disintegration of a continuous network of "lakes and channels" occurs. Furthermore, it does not depend on the detailed physico-chemical nature of the system or its composition. This universal constant depends only on the dimensionality of space. To within a few percent, this constant is found to be 0.16 for 3-dimensional lattices (62). We therefore write that:

$$\frac{V_f}{V}(T_g) = \frac{V - V^0}{V} = 0.16 \qquad \text{(A1)}$$

where V^0 is the hypothetical volume occupied by the molecules at T = 0 K.

By definition, the thermal expansion coefficient of a system, α, is $\alpha = 1/V(dV/dT)_p$.

Integrating this expression over the temperature range 0 to T_g(K) gives:

$$V = V^0 \exp[\langle\alpha\rangle T_g] \approx V^0(1 + \langle\alpha\rangle T_g) \qquad \text{(A2)}$$

where $\langle\alpha\rangle = 1/T_{go}\int^{T_g} \alpha\, dT$ is the average thermal expansion coefficient.

Substituting Eq. A2 into Eq. A1, we arrive at a simple universal relation between the glass transition temperature and the average thermal expansion coefficient:

$$\langle\alpha\rangle T_g = 0.19 \qquad \text{(A3)}$$

The molar volume of a binary mixture is:

$$V = x_1V_1 + x_2V_2 + V^E \qquad \text{(A4)}$$

where x_1 and x_2 are the mole fractions of water (for example) and a solute, V_1 and V_2 are the molar volumes of the pure components and V^E is the excess molar volume of the mixture. Differentiation of Eq. A4 with respect to temperature gives:

$$\alpha = \varphi_1\alpha_1 + \varphi_2\alpha_2 + \varphi^E\alpha^E \qquad \text{(A5)}$$

where φ_1 and φ_2 are the apparent volume fractions, $\varphi_1 = x_1V_1/V$ and $\varphi_2 = x_2V_2/V$, α_1 and α_2 are the thermal expansion coefficients of the pure components (e.g., pure water and solute), and $\varphi^E = V^E/V$ and $\alpha^E = 1/V^E(dV^E/dT)_p$ are the excess volume fraction and the excess thermal expansion coefficient, respectively. By applying Eq. A3 to pure water and a pure solute we obtain:

$$\langle\alpha_1\rangle = \frac{0.19}{T_{g1}} \text{ and } \langle\alpha_2\rangle = \frac{0.19}{T_{g2}} \qquad \text{(A6)}$$

where T_{g1} and T_{g2} are the glass transition temperatures of pure water and the pure solute, respectively. Combining Eqs. A3, A5, and A6, we arrive at the desired relation for the glass transition temperature of the mixture:

$$\frac{1}{T_g} = \frac{\varphi_1}{T_{g1}} + \frac{\varphi_2}{T_{g2}} + \frac{1}{0.19}\varphi^E\langle\alpha^E\rangle \qquad \text{(A7)}$$

Generalization of this relation to a mixture containing n components is straightforward:

$$\frac{1}{T_g} = \sum_{i=1}^{n}\frac{\varphi_i}{T_{gi}} + \frac{1}{0.19}\varphi^E\langle\alpha^E\rangle \qquad \text{(A8)}$$

where $\langle\alpha^E\rangle$ is the excess thermal expansion coefficient for a multicomponent mixture.

Equations A2–A8 rely on a crucial approximation (in addition to assuming that the glass transition is purely governed by free volume effects). To calculate $\langle\alpha^E\rangle$ between T = 0 and T_g(K), volumetric liquid data for $T > T_g$ is extrapolated to sub-T_g temperatures. That is, a hypothetical liquid behavior is assumed for $T < T_g$.

The calculation of apparent volume fractions for the components requires the mixture molar volume. The excess molar volume of a binary mixture can be expressed as:

$$V^E = \frac{x_1M_1 + x_2M_2}{\rho(x_i,T)} - (x_1V_1 + x_2V_2) \qquad \text{(A9)}$$

where $\rho(x_i, T)$ is the density of the mixture, and x_i and M_i are the mole fraction and molecular weight of component i, respectively.

The apparent volume fractions, φ_i, contain the quantities V and V_i, which are functions of temperature. Equation A7

requires knowledge of these temperature dependencies. Unfortunately, there are experimental difficulties in measuring the density of aqueous solutions at temperatures approaching the glass transition. Many of these solutions are metastable. The time-dependent crystallization of one or more of the components causes measurable changes in the density. This requires the use of an extrapolation technique for temperatures below −15°C when using our data.

The molar volume of solute i, V_i, as a function of temperature t(°C) was determined by an equation of the form:

$$V_i = \frac{V_{i,20°C}}{\left(1 - \left(\frac{0.19}{T_{gi}}\right)(t - 20°C)\right)} \quad \text{(A10)}$$

where $V_{i,20°C}$ was obtained by extrapolating solution molar volume data at 20°C to that of the pure solute. The density of supercooled water above −34°C is available (63).

The simplest way to apply this model to a given system is to use density data to determine the molar volume of the mixture, V, at each temperature. A least-squares linear fit is then used to linearly fit the V data. The V_i for each solute can be determined as a function of temperature using Eq. A10. The V_i for the solvent (in our case, water) is determined from available density data. The lowest temperature for which density data are available for supercooled water is −34°C; we use the density (64) of low-density amorphous ice (0.94 g/cm^3) to linearly interpolate between −34°C and the T_g of pure water (−136°C). The volumetric data are then used to calculated φ_i for every component at each temperature. Equation A8 (without the excess term) is transformed to the objective function F(T):

$$F(T) = \frac{1}{T} - \sum_{i=1}^{n} \frac{\varphi_i(T)}{T_{gi}} \quad \text{(A11)}$$

where

$$F(T_g) = 0 \quad \text{(A12)}$$

A rigorous application of this model requires volumetric data over a range of temperatures. An alternative technique can be used for predicting the T_g of systems using only the knowledge of the molar volume at a single temperature. It is based on the assumption that the molar volume is linear with temperature. Each set of complete V(T) data for a given concentration, x, is fit to a line using a least-squares method. The slope each of these lines is $(dV/dT)_x$. These data are then used to develop a relation between x and $(dV/dT)_x$. Then, for a given concentration, the molar volume at a temperature T is:

$$V(x, T) = V(x, T') + \left(\frac{dV}{dT}\right)_x (T - T') \quad \text{(A13)}$$

where $V(x, T')$ is the known molar volume of the mixture at T'.

APPENDIX B

Couchman and Karasz (41) have presented a model that uses classical thermodynamics to predict the composition dependence of T_g. This model treats the glass transition as an Ehrenfest second order transition in which the enthalpy, entropy and volume of the mixture are continuous at T_g. The continuity of the entropy at such a transition forms the basis of their model.

The total entropy of a binary mixture can be written as:

$$S = x_1 S_1 + x_2 S_2 - R(x_1 \ln x_1 + x_2 \ln x_2) + \Delta S_{mix} \quad \text{(B1)}$$

where x_1 and x_2 are the mole fractions and S_1 and S_2 are the molar entropies of the two components, R is the universal gas constant, and ΔS_{mix} includes all excess entropy changes associated with mixing. Expressing the entropy of the mixture at its glass transition temperature, T_g, in terms of heat capacities gives:

$$S(T_g) = x_1\left\{S_1^0 + \int_{T_{g1}}^{T_g} \frac{C_{p1}}{T}\,dT\right\} + x_2\left\{S_2^0 + \int_{T_{g2}}^{T_g} \frac{C_{p2}}{T}\,dT\right\} - R(x_1 \ln x_1 + x_2 \ln x_2) + \Delta S_{mix} \quad \text{(B2)}$$

where S_1^0 and S_2^0 are the molar entropies of the pure components at their respective glass transition temperatures, T_{g1} and T_{g2}. The entropy continuity principle is established by writing Eq. B2 for both the supercooled liquid and the glass. The simplest case, in which ΔS_{mix} is solely configurational, implies that ΔS_{mix} is also continuous at T_g. This gives:

$$x_1\left\{\int_{T_{g1}}^{T_g} \frac{C_{p1}^l}{T}\,dT\right\} + x_2\left\{\int_{T_{g2}}^{T_g} \frac{C_{p2}^l}{T}\,dT\right\} = x_1\left\{\int_{T_{g1}}^{T_g} \frac{C_{p1}^g}{T}\,dT\right\} + x_2\left\{\int_{T_{g2}}^{T_g} \frac{C_{p2}^g}{T}\,dT\right\} \quad \text{(B3)}$$

where the l and g superscripts indicate the supercooled liquid and glass states, respectively. Combining terms gives:

$$x_1\left\{\int_{T_{g1}}^{T_g} \frac{C_{p1}^l - C_{p1}^g}{T}\,dT\right\} + x_2\left\{\int_{T_{g2}}^{T_g} \frac{C_{p2}^l - C_{p2}^g}{T}\,dT\right\} = 0 \quad \text{(B4)}$$

The integrals of Eq. B4 are easily evaluated if it is assumed that each $\Delta C_{pi} = C_{pi}^l - C_{pi}^g$ is independent of temperature, which gives the following analytical expression for T_g:

$$\ln \frac{T_g}{T_{g1}} = \frac{x_2 \Delta C_{p2} \ln\left(\frac{T_{g2}}{T_{g1}}\right)}{x_1 \Delta C_{p1} + x_2 \Delta C_{p2}} \quad \text{(B5)}$$

Typically, the glass transition temperature of each pure component, T_{gi}, and the finite discontinuity in its heat capacity at T_g, ΔC_{pi}, are calorimetrically determined.

ACKNOWLEDGMENTS

This material is based upon work supported by the National Science Foundation. H.R. Corti gratefully acknowledges the financial support of Fundación Antorchas. The authors thank R. Anderson and E. Coker for their solubility and viscosity measurements, respectively. We thank S. Shamblin of the University of Wisconsin Department of Pharmacy for providing us with the freeze-dried trehalose samples. We would also like to thank the anonymous reviewers for their instructive comments.

REFERENCES

1. A. D. Elbein. *Chem. Biochem.* **30**:227–256 (1974).
2. T. E. Honadel and G. J. Killian. *Cryobiology* **25**:331–337 (1988).
3. J. S. Clegg. *Comp. Biochem. Physiol.* **14**:135–143 (1965).

4. L. M. Crowe, R. Mouradian, J. H. Crowe, S. A. Jackson, and C. Womersley. *Biochim. Biophys. Acta* **769**:141–150 (1984).
5. J. H. Crowe, L. M. Crowe, and S. A. Jackson. *Arch. Biochem. Biophys.* **220**:477–484 (1983).
6. B. J. Roser. US Patent 4,891,319, Protection of Proteins and the Like, Jan. 2, 1990.
7. B. J. Roser. US Patent 5,149,653, Preservation of Viruses, Sep. 22, 1992.
8. L. M. Crowe, J. H. Crowe, A. Rudolph, C. Womersley, and L. Appel. *Arch. Biochem. Biophys.* **242**:240–247 (1985).
9. J. L. Green and C. A. Angell. *J. Phys. Chem.* **93**:2880–2882 (1989).
10. J. H. Crowe, S. B. Leslie, and L. M. Crowe. *Cryobiology* **31**:355–366 (1994).
11. M. C. Donnamaria, E. I. Howard, and J. R. Grigera. *J. Chem. Soc. Faraday Trans.* **90**:2731–2735 (1994).
12. B. R. Rudolph, I. Chandrasekhar, B. P. Gaber, and M. Nagumo. *Chem. Phys. Lipids* **53**:243–261 (1990).
13. J. H. Crowe. *American Naturalist* **105**:563–573 (1971).
14. S. J. Webb. Bound Water in Biological Integrity, C. C. Thomas, Springfield, Illinois, 1965.
15. J. H. Crowe, L. M. Crowe, and R. Mouradian. *Cryobiology* **20**:346–356 (1983).
16. S. H. Gaffney, E. Haslam, T. H. Lilley, and T. R. Ward. *J. Chem. Soc., Faraday Trans. I* **84**:2545–2552 (1988).
17. B. J. Aldous, A. D. Auffret, and F. Franks. *Cryo-Letters* **16**:181–186 (1995).
18. R. V. Jasra and J. C. Ahluwalia. *J. Chem. Thermodynamics* **16**:583–590 (1984).
19. L. Slade and H. Levine. *Appl. Chem.* **60**:1841–1864 (1988).
20. M. Mathlouthi and A. Seuvre. *J. Chem. Soc., Faraday Trans. I* **84**:2641–2650 (1988).
21. M. Portmann and G. Birch. *J. Sci. Food Agric.* **69**:275–281 (1995).
22. S. Galema and H. Høiland. *J. Phys. Chem.* **95**:5321–5326 (1991).
23. G. G. Birch and S. Catsoulis. *Chemical Senses* **10**:325–332 (1985).
24. S. Shamil, G. G. Birch, M. Mathlouthi, and M. N. Clifford. *Chemical Senses* **12**:397–409 (1987).
25. F. Shahidi, P. G. Farrell, and J. T. Edward. *J. Solution Chem.* **5**:807–816 (1976).
26. H. Nicolajsen and A. Hvidt. *Cryobiology* **31**:199–205 (1994).
27. E. Y. Shalaev and F. Franks. *J. Chem. Soc. Faraday Trans.* **91**:1511–1517 (1995).
28. Y. Roos. *Carbohydr. Res.* **238**:39–48 (1993).
29. A. Saleki-Gerhardt and G. Zografi. *Pharm. Res.* **11**:1166–1173 (1994).
30. G. Scatchard, P. T. Jones, and S. S. Prentiss. *J. Am. Chem. Soc.* **54**:2676–2690 (1932).
31. J. Timmermans. Elsevier Publishing Co., Inc., New York, 1950.
32. William Elmer Forsythe (ed.). Smithsonian Physical Tables, 9th rev. ed., Washington D.C., Smithsonian Institution, 1956.
33. A. P. MacKenzie. *Phil. Trans. R. Soc. Lond. B.* **278**:167–189 (1977).
34. F. E. Young, F. T. Jones, and H. J. Lewis. *J. Phys. Chem.* **56**:1093–1096 (1952).
35. F. E. Young and F. T. Jones. *J. Phys. Coll. Chem.* **53**:1334–1338 (1949).
36. F. E. Young. *J. Phys. Chem.* **61**:616–620 (1957).
37. L. Slade and H. Levine. *Critical Reviews in Food Science and Nutrition* **30**:115–360 (1991).
38. D. R. Lide (ed.). CRC handbook of Chemistry and Physics, 71st ed., Boca Raton, FL, CRC Press, Inc., 1990.
39. S. Shamblin, University of Wisconsin Department of Pharmacy, personal communication, 1996.
40. A. Kolker, D. Miller, and J.J. de Pablo. Proceedings of the annual conference of the American Institute of Chemical Engineers, November 1995, Miami, FL.
41. P. R. Couchman and F. E. Karasz. *Macromol.* **11**:117–119 (1978).
42. M. Sugisaki, H. Suga, and S. Seki. *Bull. Chem. Soc. Jpn.* **41**:2591–2599 (1968).
43. M. G. Sceats and S. A. Rice. F. Franks (ed.), Water: A Comprehensive Treatise, Vol. .7, Plenum Press, New York, 1982, pp. 90–98.
44. G. P. Johari. *Philosophical Mag. B* **35**:1077–1090 (1977).
45. A. Hallbrucker, E. Mayer, and G. P. Johari. *J. Phys. Chem.* **93**:4986–4990 (1989).
46. C. A. Angell and J. C. Tucker. *J. Phys. Chem.* **84**:268–272 (1980).
47. C. A. Angell. *Ann. Rev. Phys. Chem.* **34**:593–630 (1983).
48. A. Hallbrucker, E. Mayer, and G. P. Johari. *Phil. Mag. B* **60**:179–187 (1989).
49. R. J. Speedy, P. G. Debenedetti, R. S. Smith, C. Huang, and B. D. Kay. *J. Chem Phys.* **105**:240–244 (1996).
50. M. L. Williams, R. F. Landel, and J. D. Ferry. *J. Am. Chem. Soc.* **77**:3701–3707 (1955).
51. C. A. Angell. *J. Non-Crystalline Solids* **131–133**:13–31 (1991).
52. T. Soesanto and M. C. Williams. *J. Phys. Chem.* **85**:3338–3341 (1981).
53. S. R. Elliot. Physics of Amorphous Materials, Second Edition, John Wiley and Sons, Inc., New York, 1990.
54. R. J. Bellows and C. J. King. *AIChE Symposium Series* **69**:33–41 (1973).
55. C. A. Angell, R. D. Bressel, J. L. Green, H. Kanno, M. Oguni, and E. J. Sare. *J. Food Eng.* **22**:115–142 (1994).
56. G. Blond. *Cryo-Letters* **10**:299–308 (1989).
57. H. Kawai, M. Sakurai, Y. Inoue, R. Chûjô, and S. Kobayashi. *Cryobiology* **29**:599–606 (1992).
58. Y. Roos. *Carbohydr. Res.* **238**:39–48 (1993).
59. Y. Dakhnovskii and V. Lubchenko. *J. Chem. Phys.* **104**:664–668 (1996).
60. D. P. Miller, J. J. de Pablo, and H. R. Corti. *J. Chem. Phys.* **105**:8979–8980 (1996).
61. G. Fleissner, A. Hallbrucker, and E. Mayer. *J. Phys. Chem.* **97**:4806–4814 (1993).
62. R. Zallen. The Physics of Amorphous Solids, John Wiley & Sons, Inc., New York, 1983.
63. B. V. Zheleznyi. *Russ. J. Phys. Chem.* **43**:1311–1312 (1969).
64. P. H. Poole, U. Essmann, F. Sciortino, and H. E. Stanley. *Physical Review E* **48**:4605–4610 (1993).
65. L. Her and S. L. Nail. *Pharm. Res.* **11**:54–59 (1994).
66. M. Gordon and J. Taylor. *J. Appl. Chem.* **2**:493–500 (1952).
67. A. Saleki-Gerhardt. Ph.D. Thesis, University of Wisconsin-Madison, 1993.